The relationship between fluid injection volumes and uncontrolled fracture ascent.

Timothy Davis[1], Eleonora Rivalta[1], Torsten Dahm[1]

[1]GFZ (GeoForschungsZentrum), Physics of Earthquakes and Volcanoes, Helmholtzstraße 6/7, Building H 7, 14467 Potsdam. {davis,rivalta,dahm}@gfz-potsdam.de

ABSTRACT

Hydro-fracturing is a routine industrial technique whose safety depends on fractures remaining confined within the target rock volume. Both observations and theoretical models show that pockets of fluid can propagate large distances in the Earth's crust, in a self-sustained, uncontrolled manner, providing that the fluid volume is large enough. Existing models that describe when self-sustaining ascent starts are difficult to use for predictions, as they are mostly two-dimensional (2D) and depend on parameters (typically the fracture length) that are hard to assess, even a posteriori. Here we constrain, both analytically and numerically in three-dimensions (3D), scale-independent critical volumes as a function of only rock and fluid properties. We apply our model to laboratory, industrial and natural settings, showing that our critical volumes are consistent with observations and can be used as a conservative estimate in geological applications. We find typical injection volumes exceed the limit we define for the start of self-sustaining fracture ascent. We describe a number of other processes that may work to arrest fractures with volumes exceeding this limit. This appears to have resulted in a false sense of operational safety when working with large injection volumes. In

the context of our findings we outline the quantitative work that would be required to better elucidate the processes causing fracture arrest, which could help to assess more comprehensively the safety of such operations.

INTRODUCTION

Official guidelines for hydraulic fracturing (EPA, 2016; Mair et al., 2012) outline safe operational practices for regulators. Such reports often state that during routine operations fractures are unlikely to grow out of the target rock formation, as typical injection pressures are too low for this to occur. These claims are substantiated with empirical observations from closed access microseismic data of scarce vertical fracture growth following injection (Fisher and Warpinski, 2012). Evidence for unsafe vertical migration of such fluids remains ambiguous (Vidic et al., 2013).

Natural analogues of fluid migration by hydro-fracturing include drainage crevasses in melting glaciers and magma transport by dyking. Field and experimental observations provide some indication of typical rates of fracture ascent, in the order of mm/s to around half a m/s. (Das et al., 2008; Tolstoy et al., 2006). For water-filled fractures in rock this has not been observed; estimates from geochemical analysis supply similar rates of ~0.01-0.1 m/s, (1 km/day) (Okamoto and Tsuchiya, 2009). Theoretical arguments suggest that the migration velocity should have a dependency on volume (Dahm, 2000; Heimpel and Olson, 1994).

According to theory, tip-propagation occurs when a critical amount of fluid has accumulated inducing enough stress to overcome the medium's fracture toughness, K_c (Secor and Pollard, 1975). So far, critical 'volumes' are given in terms of the fracture length, which is not directly observable and difficult to estimate from observations (Dahm, 2000; Secor and Pollard, 1975; Taisne et al., 2011); moreover, such analyses have been carried out in 2D only, not capturing the fracture's 3D shape and scaling of volume vs length.

Here, after deriving a theoretical model and validating it with numerical simulations, we apply this to cracks filled with air, water, oil and magma in solids of varying stiffness and toughness, across a wide range of length scales.

METHODS

Hydrofracturing and stress gradients

[Figure 1 about here.]

We consider a pressurised penny-shaped crack of radius c and volume V in an elastic medium. The crack can only grow when the stress intensity K_I at its tip-line exceeds K_c. The elastic parameters of the medium (shear modulus, μ, and Poisson's ratio, ν) control the fracture's aperture. The internal pressure p_0 must overcome the stress normal to the crack walls (generally the minimum compressive stress, σ_{min}) by an amount accommodating the volume V against the elastic forces, Fig. 1A/B.

When the crack is vertical, the gradient in the normal stress acting to close the crack and the gradient in the load due to the overlying fluid acting to open the crack, i.e. $\rho_r g$ and $\rho_f g$ in Fig. 1A, where ρ_r and ρ_f are the densities of the host rock and fluid, respectively, result in a net stress gradient $\Delta\gamma$ acting to push open the crack walls in an inverse 'teardrop' shape, Fig. 1B/C. When the crack is inclined $\Delta\gamma$ needs to be adjusted by $cos(\theta)$, where θ is the cracks' angle away from vertical. Quantitative formulations used to assess industrial fracture heights neglect stress gradients e.g. Xu et al. (2019); Yue et al. (2019). This contrasts with routine observations of stress gradients from industry data (Fig. 1A) and the fact that these gradients are considered in the well design of industrial operations (Lecampion et al., 2013; Mair et al., 2012). When this gradient is included in formulations, stress intensity varies around the fracture's tip-line (Fig. 2). Where K_c is exceeded, the upper tip-line advances. The contained fluid flows into this newly created fracture surface while the bottom edge of the fracture is pinched shut as the internal pressure drops. With a great enough volume this fluid movement maintains a critically stressed upper tip-line and the fracture reaches a state of 'self-sustaining propagation'. Fluid viscosity will cause some fluid to stay trapped in the tail trailing behind the fracture; if fluid viscosity is low enough, the contained fluid is virtually all transported. Provided the fracture's shape and volume are maintained, no additional forces, such as pressure from injection, are required to aid this state of propagation.

Analytical formulation

Secor and Pollard (1975) define in 2D the size and pressure inside a vertical fracture subject to $\Delta\gamma = (\rho_r - \rho_f)g$ such that at the upper tip $K_I^+ = K_c$ and at the lower tip $K_I^- = 0$. They assume that the crack is filled with incompressible inviscid (uniform fluid pressure) fluid and sits within an infinite homogeneous linear elastic medium; where both the fluid and rock have a uniform density. We adapt this formulation to 3D (see Supplementary Material), finding the pressure and size of a penny-shaped crack where the stress intensity at the top is equal to the fracture toughness and the fractures basal tip is bordering on closure, the rest of the tip-line is sub-critically stressed (Fig. 1b and c). We then convert this size and internal pressure to the volume of fluid inside this penny-shaped fracture:

$$V_c^{an} = \frac{(1-\nu)}{16\mu}\left(\frac{9\pi^4 K_c^8}{\cos(\theta)\Delta\gamma^5}\right)^{1/3}. \tag{1}$$

This equation for the critical volume before self-sustaining ascent, requires validation in order to evaluate the bias due to approximating the shape of the propagating crack as circular (Fig. 1D/E).

[Figure 2 about here.]

Numerical model

To simulate propagation, we use a 3D Boundary Element program where each element is a triangular dislocation with constant displacement (Fig. 2). We start the simulation with a vertical penny-shaped crack. We fix the number of elements, K_c, $\Delta\gamma$, μ, ν and the volume of fluid, V. We set the initial radius to 0.4c, where c is the analytical critical crack radius, derived in the Supplementary Material. In our 350+ simulations we use variables spanning several orders of magnitude: G=190–5·10^{10}·Pa, ν=0.25–0.49, $\Delta\gamma$=7.8·10^2–2.2·10^4·Pa·m^{-1} and K_c=1-1·10^8·Pa·m$^{0.5}$. We state the fracture has reached self-sustaining ascent when its upper tip has travelled $4c$ upwards. Our numerical method assumes an inviscid fluid. During each iteration the critically stressed portions of the tip-line advance proportionally to the local value of K_I/K_c. For a full description of the numerical methods, accuracy and results, see the Supplementary Material.

For all simulations, independent of mesh sampling, we find that if $V = 0.7V_c^{an}$ the numerical code returns a trapped fracture and if $V = 0.8V_c^{an}$ the fracture always reaches self-sustaining propagation. Therefore, scaling Eq. 1 by 0.75 supplies the numerical estimate of V_c, independent of the scale we use:

$$V_c^{num} = \frac{3(1-\nu)}{64\mu}\left(\frac{9\pi^4 K_c^8}{\cos(\theta)\Delta\gamma^5}\right)^{1/3}. \tag{2}$$

APPLICATIONS

Analog gelatine experiments

[Figure 3 about here.]

The analog study of Heimpel and Olson (1994) inspects critical volumes of fluids ascending in gelatine blocks of different stiffness and fracture toughness (Fig. 3). The slope of volume vs speed from their experimental results shows an obvious increase in speed past a certain volume that may indicate the transition away from the sub-critical propagation regime. Heimpel and Olson (1994) interpret the transition away from sub-critical propagation at crack-tip velocities of ∼0.7 cm/s, crosses in Fig. 3. Using ρ_r=1000 kg·m^{-3}, ν=0.5 and setting μ, ρ_f and K_c to match their experiments, we find that our value of V_c^{num} captures the transition described above. This result shows our equation works can describe observations for idealised experimental data.

Magmatic dykes

We consider magma propagation volumes at Piton de la Fournaise, La Réunion, to see how our equation matches observed dyke volumes. Among the dyke intrusions observed between 1998-2016, the smallest volume inferred from crustal deformation data is 0.05·10^6·m^3 (Fukushima et al., 2010). Using $\rho_r - \rho_f$=100 kg·m^{-3}, μ=5 GPa, ν=0.25 (Fukushima et al., 2010) and K_c ranging from 29 to 112 MPa·$m^{1/2}$ (Delaney and Pollard, 1981), we retrieve V_c^{num}=0.05·10^6 and 2·10^6·m^3, respectively. These critical volumes are consistent with that of the minimum observed dyke size. As such our approximation predicts the correct scale in natural settings, provided K_c values estimated from field data are used.

Water injection into stiff rock

The UK government defines hydraulic fracturing as operations that use over 1,000 m^3 of fluid per frack stage. During a hydro-fracturing procedure, proppant is injected in the final phase to maintain an open fracture (e.g. spherical quartz grains). After the operation, not all injected fluid is recovered when the wellhead valve is opened: Vidic et al. (2013) report an average of only 10% fluid recovery in flowback waters, noting that this recovery volume decreases when shut-in times are longer. Using ρ_r=2700 kg·m^{-3}, ρ_f=1000 kg·m^{-3}, μ=8.9 GPa, ν=0.25 and K_c in the range 0.36–4.05 to 7–25 MPa·$m^{1/2}$, we obtain $V_c^{num} = 6{\cdot}10^{-2}$ and 500 m^3 respectively. These K_c values are for laboratory-sized shale samples from 100 to 1000 m confining pressure and effective K_c values estimated for veins in the field, respectively (Gehne et al., 2020; Olson, 2003). Current operations use volumes around double our highest predicted limit. Few observations attest to the fact that industrial operations can cause ascent of fluids in fractures. One such example, are the spectacular surface fissures created due to steam injection documented in Schultz (2016); additional examples can be found in Schultz et al. (2016). Geochemical data from aquifers above fracking operation sites has shown some evidence of the contamination of overlying units, which is attributed to poor well casing design, rather than fracture ascent (Vidic et al., 2013). Usually, microseismic monitoring of actual fracking operations show limited vertical extents of the fractures, however, these data are proprietary and methodological descriptions are scarce (Fisher and Warpinski, 2012). Experimental fracturing data is of little help as volumes injected are typically below or close to our volumetric limit, with injected volumes of 2 to 20 m^3 (Pandurangan et al., 2016; Warpinski et al., 1982).

Natural degassing, such as CO_2 in the Cheb basin, Czech Republic, has chemical signatures of fluids that have ascended over 20 km through the crust (Weinlich, 2014). This migration is hard to explain by deep vertically extensive permeable zones. Supercritical CO_2 at depth has a similar density to water, and as such may be a good natural analog for water filled fracture ascent. We saw that in analogue and magmatic examples Eq. 2 predicts the correct order of magnitude of critical volumes; at the same time, it appears that this equation is conservative for high volume water injection as fracture ascent in these settings has rarely been observed.

DISCUSSION AND CONCLUSIONS

In summary, Eq. 2 provides an estimate of the minimum fluid volume for self-sustained propagation of fluid-filled fractures, ranging from cm to tens of km. V_c is dependent on $K_c^{8/3}$; since K_c is often poorly constrained V_c suffers from large uncertainties. Values of K_c obtained in laboratory experiments show a strong dependency on pressure and temperature. Field estimates of effective K_c from trapped fractures can be orders of magnitude larger. An effective way to estimate K_c in Eq. 2 incorporating all processes affecting the energy needed to extend the fracture at different scales would clearly be beneficial for any fracture mechanics based analysis of rock masses and the resultant interpretations.

In our derivation we have neglected the effects of viscosity. Whether these effects will dominate over toughness in determining fracture growth can be assessed by evaluating the time scale needed for the fluid pressure to equilibrate within the crack, as this will mean that viscous dissipation is low and crack growth will be toughness-dominated (Bunger and Detournay, 2007). The model of Bunger and Detournay (2007) assumes a constant injection rate with no stress gradients, we assume this still provides a rough estimate of the timescale until this transition. Typical industrial operations use fluid viscosity of 0.0005–0.001 Pa·s, injection rates between 0.5–10 mbut^3/min and stiffness of 10–

40 GPa. Using low values of K_c from laboratory experiments in shale, 0.36 MPa·m$^{1/2}$, this transition time ranges between 10 seconds to times exceeding the end of injection. Whereas, setting K_c higher, values for shale at depth, e.g. 4 MPa·m$^{1/2}$ this significantly reduces this range to below milliseconds to a maximum of 1 minute. This suggests that, depending on K_c, Eq. 2 can be a relevant estimate of V_c^{num}, independent of viscous forces.

[Figure 4 about here.]

While theory and experiments support Eq. 2, this appears to be overly conservative in practice, as injections of quantities of fluid exceeding this do not result in significant ascent in most cases. In part, this discrepancy results from our simplification of the process, as mass conserving propagation in a homogeneous linear-elastic medium. Fig. 4 shows a schematic of processes not quantified in relation to critical fluid volumes which we review in detail below.

1. A series of mechanisms can reduce V during propagation and thus promote crack arrest. These include leak-off from the fractures faces, the fracture becoming multistranded/compartmentalised, fluid recovery (extraction), or fluid remaining in the tail of the fracture due to added proppant or viscous forces (Taisne and Tait, 2009).

2. Mechanisms that can lead to an effective increase of K_c, and thus also promote crack arrest, include plastic tip processes, the fracture entering in a zone of damage of the host rock (Kaya and Erdogan, 1980; Sih et al., 1965) or seismicity surrounding the fracture, causing reduction in the system's energy/blunting the fracture's tip (Rivalta et al., 2015).

3. Heterogeneous μ or K_c or stress barriers may also lead to arrest of fractures by deflection or promoting lateral growth (Bunger and Lecampion, 2017; Maccaferri et al., 2011; Warpinski et al., 1985),

4. Eq. 2 has a clear dependency on the fracture's dip. If the minimum compressive stress is vertical, this promotes flat lying fractures.

Quantification of processes acting to halt fracture ascent, especially in the context of the variables in our equation, are critical to understand which volumetric limits can be deemed safe. In particular, the gradient in stress with depth must be included to assess this process. Without such quantification, regulation of this industrial process will continue to rely on empirical evidence for safe rates, volumes and depths from select operations that may not be representative.

ACKNOWLEDGEMENTS

T.D. is funded by the DFG-ICDP grant N. RI 2782/3-1.

References

Bell, J., Price, P., and McLellan, P. (1990). In-situ stress in the western canada sedimentary basin. *Bulletin of Canadian Petroleum Geology*, 38(1):157–157.

Bunger, A. and Detournay, E. (2007). Early-time solution for a radial hydraulic fracture. *Journal of engineering mechanics*, 133(5):534–540.

Bunger, A. and Lecampion, B. (2017). Four critical issues for successful hydraulic fracturing applications. Technical report, CRC Press.

Dahm, T. (2000). On the shape and velocity of fluid-filled fractures in the earth. *Geophysical Journal International*, 142(1):181–192.

Das, S. B., Joughin, I., Behn, M. D., Howat, I. M., King, M. A., Lizarralde, D., and Bhatia, M. (2008). Fracture propagation to the base of the greenland ice sheet during supraglacial lake drainage. *Science*, 320(5877):778–781.

Delaney, P. T. and Pollard, D. D. (1981). Deformation of host rocks and flow of magma during growth of minette dikes and breccia-bearing intrusions near ship rock, new mexico. Technical report, USGPO.

EPA, U. (2016). Hydraulic fracturing for oil and gas: Impacts from the hydraulic fracturing water cycle on drinking water resources in the united states. *Washington, DC: US Environmental Protection Agency, EPA/600/R-16/236F*.

Fisher, M. K. and Warpinski, N. R. (2012). Hydraulic-fracture-height growth: Real data. *SPE Production & Operations*, 27(01):8–19.

Fukushima, Y., Cayol, V., Durand, P., and Massonnet, D. (2010). Evolution of magma conduits during the 1998–2000 eruptions of piton de la fournaise volcano, réunion island. *Journal of Geophysical Research: Solid Earth*, 115(B10).

Gehne, S., Forbes Inskip, N., Benson, P., Meredith, P., and Koor, N. (2020). Fluid-driven tensile fracture and fracture toughness in nash point shale at elevated pressure. *Journal of Geophysical Research: Solid Earth*, page e2019JB018971.

Heimpel, M. and Olson, P. (1994). Buoyancy-driven fracture and magma transport through the lithosphere: models and experiments. In *International Geophysics*, volume 57, pages 223–240. Elsevier.

Kaya, A. and Erdogan, F. (1980). Stress intensity factors and cod in an orthotropic strip. *International Journal of Fracture*, 16(2):171–190.

Lecampion, B., Bunger, A., Kear, J., and Quesada, D. (2013). Interface debonding driven by fluid injection in a cased and cemented wellbore: Modeling and experiments. *International Journal of Greenhouse Gas Control*, 18:208–223.

Maccaferri, F., Bonafede, M., and Rivalta, E. (2011). A quantitative study of the mechanisms governing dike propagation, dike arrest and sill formation. *Journal of Volcanology and Geothermal Research*, 208(1-2):39–50.

Mair, R., Bickle, M., Goodman, D., Koppelman, B., Roberts, J., Selley, R., Shipton, Z., Thomas, H., Walker, A., Woods, E., and Younger, P. (2012). Shale gas extraction in the uk: a review of hydraulic fracturing.

Okamoto, A. and Tsuchiya, N. (2009). Velocity of vertical fluid ascent within vein-forming fractures. *Geology*, 37(6):563–566.

Olson, J. E. (2003). Sublinear scaling of fracture aperture versus length: an exception or the rule? *Journal of Geophysical Research: Solid Earth*, 108(B9).

Pandurangan, V., Chen, Z., and Jeffrey, R. G. (2016). Mapping hydraulic fractures from tiltmeter data using the ensemble kalman filter. *International Journal for Numerical and Analytical Methods in Geomechanics*, 40(4):546–567.

Rivalta, E., Taisne, B., Bunger, A., and Katz, R. (2015). A review of mechanical models of dike propagation: Schools of thought, results and future directions. *Tectonophysics*, 638:1–42.

Schultz, R. A. (2016). Causes and mitigation strategies of surface hydrocarbon leaks at heavy-oil fields: examples from alberta and california. *Petroleum Geoscience*, 23(2):231–237.

Schultz, R. A., Mutlu, U., and Bere, A. (2016). Critical issues in subsurface integrity. In *50th US Rock Mechanics/Geomechanics Symposium*. American Rock Mechanics Association.

Secor, D. T. and Pollard, D. D. (1975). On the stability of open hydraulic fractures in the earth's crust. *Geophysical Research Letters*, 2(11):510–513.

Sih, G. C., Paris, P., and Irwin, G. R. (1965). On cracks in rectilinearly anisotropic bodies. *International Journal of Fracture Mechanics*, 1(3):189–203.

Taisne, B. and Tait, S. (2009). Eruption versus intrusion? arrest of propagation of constant volume, buoyant, liquid-filled cracks in an elastic, brittle host. *Journal of Geophysical Research: Solid Earth*, 114(B6).

Taisne, B., Tait, S., and Jaupart, C. (2011). Conditions for the arrest of a vertical propagating dyke. *Bulletin of Volcanology*, 73(2):191–204.

Tolstoy, M., Cowen, J., Baker, E., Fornari, D., Rubin, K., Shank, T., Waldhauser, F., Bohnenstiehl, D., Forsyth, D., Holmes, R., and Love, B. (2006). A sea-floor spreading event captured by seismometers. *Science*, 314(5807):1920–1922.

Vidic, R. D., Brantley, S. L., Vandenbossche, J. M., Yoxtheimer, D., and Abad, J. D. (2013). Impact of shale gas development on regional water quality. *Science*, 340(6134):1235009.

Warpinski, N. R., Branagan, P., and Wilmer, R. (1985). In-situ stress measurements at us doe's multiwell experiment site, mesaverde group, rifle, colorado. *Journal of petroleum technology*, 37(03):527–536.

Warpinski, N. R., Schmidt, R. A., and Northrop, D. A. (1982). In-situ stresses: the predominant influence on hydraulic fracture containment. *Journal of Petroleum Technology*, 34(03):653–664.

Weinlich, F. (2014). Carbon dioxide controlled earthquake distribution pattern in the nw bohemian swarm earthquake region, western eger rift, czech republic–gas migration in the crystalline basement. *Geofluids*, 14(2):143–159.

Xu, W., Prioul, R., Berard, T., Weng, X., and Kresse, O. (2019). Barriers to hydraulic fracture height growth: A new model for sliding interfaces. In *SPE Hydraulic Fracturing Technology Conference and Exhibition*. Society of Petroleum Engineers.

Yue, K., Olson, J. E., and Schultz, R. A. (2019). The effect of layered modulus on hydraulic-fracture modeling and fracture-height containment. *SPE Drilling & Completion*.

FIGURE CAPTIONS

Figure 1: A) Stress vs depth in the crust, data from (Bell et al., 1990), crack shown in red with length $2c$. B) Stress boundary conditions and 3D crack wall displacement. C) Cross sections of crack wall displacement, itp=interpenetration.

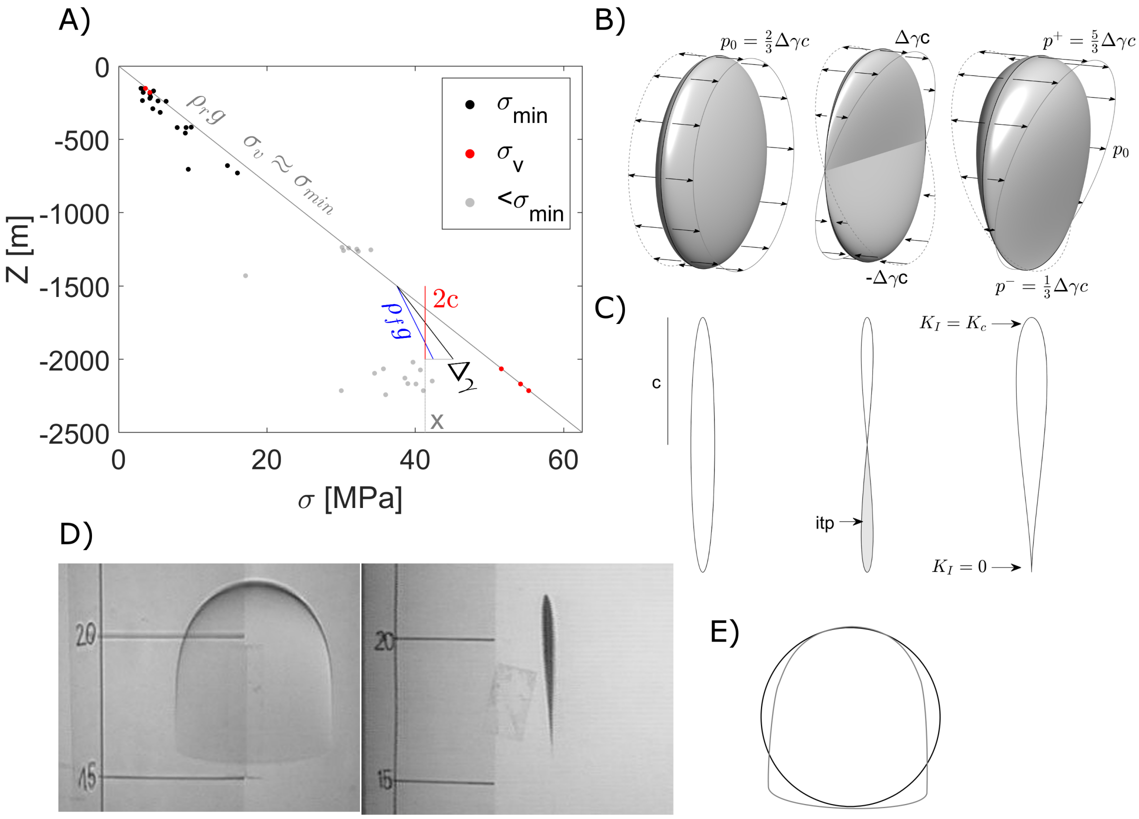

Figure 2: Numerical simulation of crack propagation (from left to right), looking at the fractures' face (left) and cross section (right). Grey points are edges that closed in the previous iteration.

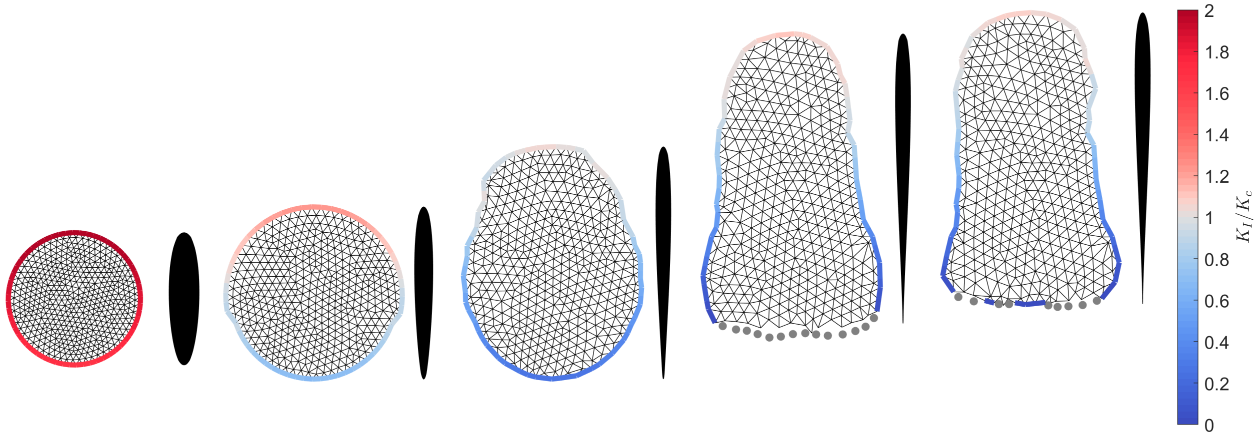

Figure 3: $V*mu$ vs K_c from (Heimpel and Olson, 1994). Eq. 2 predictions shown as black lines. The thickness of the grey filled patches represents the velocity of the crack as the volume increases, normalised by maximum observed velocity.

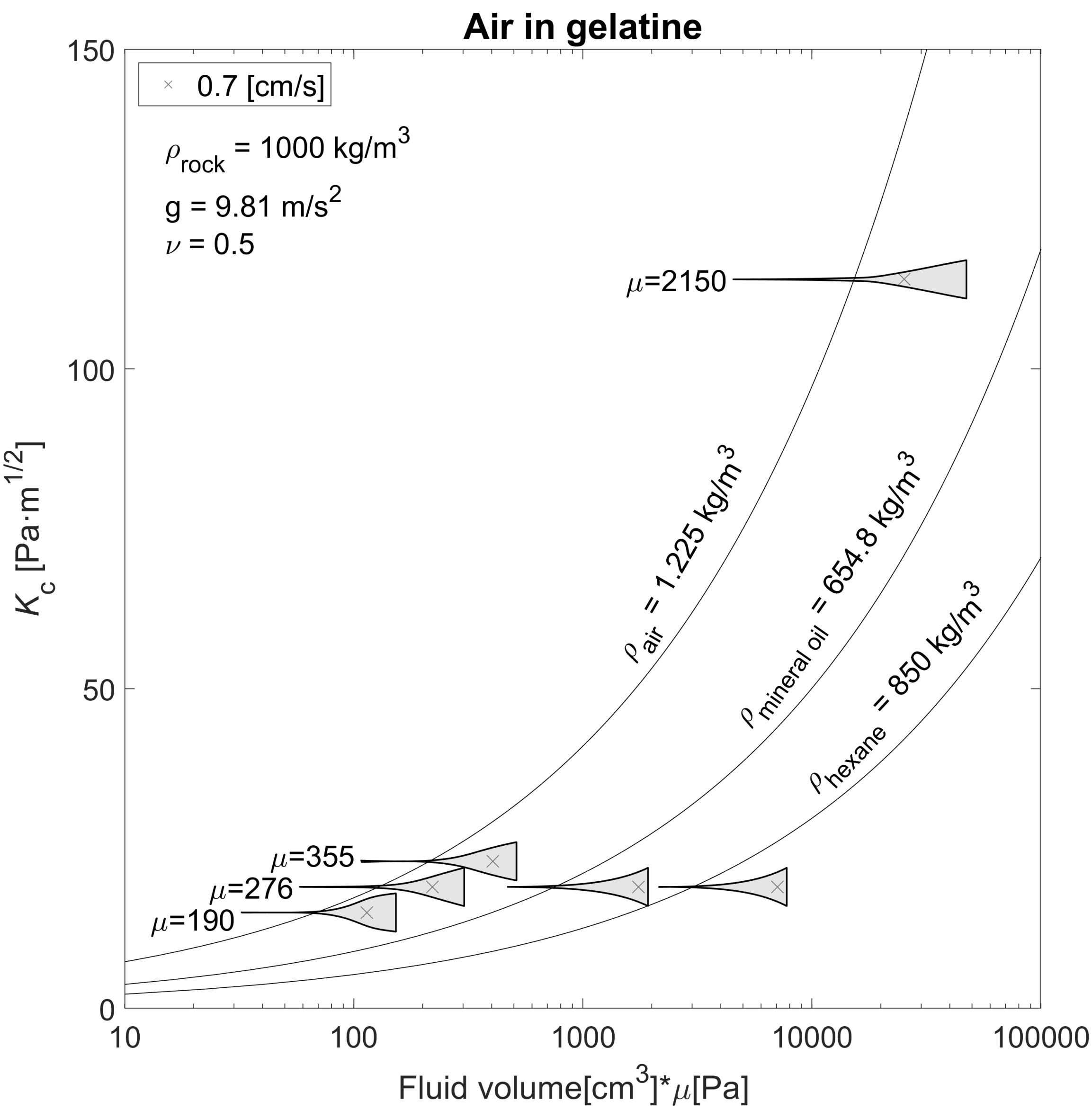

Figure 4: Processes that can hinder fracture ascent, K and V relate to effective K_c and V_c operating in Eq. 2